Preparation of C-based Magnetic Materials from Fruit Peel and Hydrochar using Snake Fruit (*Salacca zalacca*) Peel as Adsorbents for the Removal of Malachite Green Dye

Mauizatul Hasanah[1,3], Alfan Wijaya[2], Fitri Suryani Arsyad[3], Risfidian Mohadi[3], and Aldes Lesbani[2,3*]

[1]Department of Pharmacy, School of Pharmacy Bhakti Pertiwi, Jl. Ariodillah III No. 22A, Palembang 30128, South Sumatera, Indonesia
[2]Research Center of Inorganic Materials and Coordination Complexes, Faculty of Mathematics and Natural Sciences, Sriwijaya University, Jl. Padang Salasa No. 524 Ilir Barat 1, Palembang 30139, South Sumatera, Indonesia
[3]Doctoral Program, Faculty of Mathematics and Natural Sciences, Sriwijaya University, Jl. Padang Selasa No. 524 Ilir Barat 1, Palembang 30139, Indonesia

ARTICLE INFO

Received: 6 Sep 2022
Received in revised: 7 Nov 2022
Accepted: 10 Nov 2022
Published online: 23 Nov 2022
DOI: 10.32526/ennrj/21/202200192

Keywords:
Hydrothermal treatment/ Snake fruit peel/ Hydrochar/ Magnetic material/ Adsorption/ Malachite green dye

*** Corresponding author:**
E-mail:
aldeslesbani@pps.unsri.ac.id

ABSTRACT

In this study, fruit peel-based magnetic (M-Sp) and hydrochar-based magnetic (M-HSp) materials were successfully synthesized by hydrothermal and magnetization treatments. Characterization using X-ray diffraction, Fourier-transform infrared spectroscopy, vibrating sample magnetometry, and scanning electron microscopy-energy dispersive spectroscopy confirmed their successful synthesis. The materials were applied as adsorbents for the removal of malachite green (MG) dye. Equilibrium adsorption occurred at 90 min according to the PSO kinetic model, and the adsorption followed the Langmuir isotherm. The adsorption capacity of the materials was improved by the hydrothermal and magnetic treatments compared to that of the untreated initial material. The adsorption capacities of M-Sp and M-HSp were 69.444 and 88.889 mg/g, respectively. The M-Sp and M-HSp adsorbents could be reused for up to four regeneration cycles compared to the three cycles for the initial material. The adsorption mechanism of MG dye by the M-Sp and M-HSp adsorbents was suggested to occur via hydrogen bond, electrostatic, π-π, and physical interactions. The magnetic materials prepared in this study had a high adsorption capacity and adsorbent reusability, rendering them promising for use in dye removal and to facilitate separation between adsorbents and adsorbates.

1. INTRODUCTION

Snake fruit (*Salacca zalacca*) is a tropical fruit found in Southeast Asia; it is known by the name "Salak" in Indonesia (Zubaidah et al., 2018). Snake fruit peel (Sp) is an easily obtainable biomass produced from agricultural waste. As it has no market value, it has rarely been investigated and has not been widely utilized warranting further study (Yvonne et al., 2018). Previous research (Azizah and Fatimah, 2020) (Rahmayanti et al., 2022) utilizing Sp as an adsorbent to remove dyes and heavy metals reported fairly high adsorption capacity. Thus, Sp has many advantages in that it can be easily obtained and has good adsorption capabilities, rendering it promising for application as an adsorbent to eliminate waste water or organic pollutants.

The adsorption ability of Sp can be enhanced by hydrothermal treatment to obtain hydrochar. Hydrochar has been widely used as an effective adsorbent to remove dye pollutants with a high adsorption capacity (Haris et al., 2022; Hasanah et al., 2022). One of the most studied dye pollutants is malachite green (MG), which is a cationic dye and widely used in the textile, leather, and other industries; it is considered an organic pollutant in wastewater. It has been reported that the MG dye has many adverse effects on humans upon exposure owing to its high toxicity, teratogenicity, carcinogenicity and mutagenicity (Mohadi et al., 2022;

Citation: Hasanah M, Wijaya A, Arsyad FS, Mohadi R, Lesbani A. Preparation of c-based magnetic materials from fruit peel and hydrochar using snake fruit (*Salacca zalacca*) peel as adsorbents for the removal of malachite green dye. Environ. Nat. Resour. J. 2023;21(1):67-77. (https://doi.org/10.32526/ennrj/21/202200192)

Wu et al., 2022; Qiao et al., 2022). In addition, MG dye can irritate the respiratory tract, affect digestion, and cause skin problems such as rashes or swelling, as well as permanent damage to the eyes from contact (Das et al., 2021). MG dye also blocks the transmission of light, which can adversely affect the growth of aquatic organisms (Wang et al., 2022). Therefore, it is necessary to investigate methods for the removal of this dye. The adsorption method has been extensively advocated by researchers for the removal of dye pollutants owing to its simple process, low cost, and high removal efficiency (Karthi et al., 2022; Gajera et al., 2022; Alqadami et al., 2018; Dil et al., 2018).

Research conducted in recent years has particularly focused on the development of magnetic materials based on carbon to separate adsorbents from adsorbates at the end of the adsorption process (Cojocaru et al., 2019). Magnetic materials are also widely used in the removal of dye pollutants, both as adsorbents and as photocatalysts. Magnetic materials used in the removal of dye pollutants include carbon-based materials such as chitosan-magnetic Fe_3O_4/activated carbon nanocomposites that adsorb cationic and anionic dyes (Kaveh and Bagherzadeh, 2022), a chitosan-based magnetic material that could adsorb acid orange 7 dye with an adsorption capacity of 97 mg/g (Cojocaru et al., 2019), a magnetic cellulose-based ionic liquid that could adsorb MG and Congo Red dyes with adsorption capacities of 1,299.3 mg/g and 1,068.1 mg/g, respectively (Ling et al., 2022), a superb natural magnetic material that could adsorb crystal violet dye with an adsorption capacity of 117 mg/g (Sanad et al., 2021), and a biochar-based magnetic material that could adsorb rhodamine B and MG dyes with adsorption capacities of 334.89 mg/g and 576.73 mg/g, respectively (Cheng et al., 2022). Thus, carbon-based magnetic materials are promising novel adsorbents to remove dye pollutants.

In this study, Sp (from *Salacca zalacca*) which has rarely been employed in related studies was subjected to hydrothermal and magnetization treatments to improve its properties. The obtained materials were analyzed using X-ray diffraction (XRD), Fourier-transform infrared spectroscopy (FT-IR), vibrating sample magnetometer (VSM), and scanning electron microscopy with energy dispersive spectroscopy (SEM-EDS). The materials were then applied as adsorbents to remove MG dye and study the effect of the pH pzc, contact time, as well as study the adsorption isotherm, adsorption thermodynamics, and regeneration ability.

2. METHODOLOGY

2.1 Chemicals and instrumentation

The Sp used in this study was sourced from Palembang, South Sumatera, Indonesia. The chemicals used included ortho-phosphoric acid (H_3PO_4; Merck, Germany), iron(III) chloride ($FeCl_3$; Sigma Aldrich, Germany), iron(II) sulfate heptahydrate ($FeSO_4 \cdot 7H_2O$; Smart Lab, Indonesia), ammonia solution (NH_3 25%; Merck, Germany), hydrochloric acid (HCl; Mallinckrodt LabGuard, France), sodium hydroxide (NaOH; Merck, Germany), and sodium chloride (NaCl; Merck, Germany). The MG powder (cationic dye) was obtained from a textile factory in Palembang, South Sumatera, Indonesia (its chemical structure is shown in Figure 1). Distilled water was purchased from Brataco Inc., Indonesia. The material was characterized using a Rigaku Miniflex-600 X-ray diffractometer (Japan), Shimadzu Prestige-21 FTIR spectrophotometer (Japan), OXFORD VSM1.2H vibrating sample magnetometer (England), and Quanta 650 SEM-EDS apparatus (England). Absorbance measurements of the dye solution were conducted using (UV) visible Biobase spectrophotometer UV BK-1800PC (China).

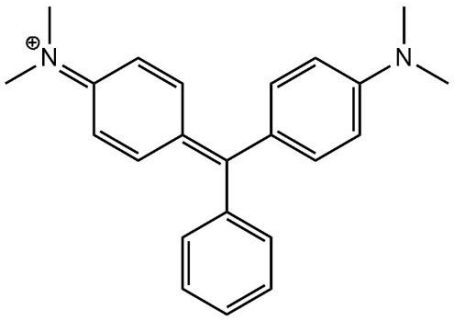

Figure 1. Chemical structure of malachite green dyes

2.2 Preparation of hydrochar from Sp

The thoroughly washed Sp was dried in the sun, ground until smooth, and filtered using a 40 mesh-sized sieve. Hydrochar from the snake fruit peel (HSp) was produced through hydrothermal carbonization treatment, which was carried out by adding as much as 2 g Sp powder to 50 mL of H_3PO_4. The solution was placed in a hydrothermal stainless steel-autoclave (volume: 100 mL), then placed in the oven for 6 h at 150°C (Çatlıoğlu et al., 2020). The mixture was subsequently filtered and washed using distilled water, and then dried in the oven for 6 h at 110°C. The initial and obtained materials were characterized using XRD, FTIR, and SEM-EDS analyses.

2.3 Preparation of fruit peel-based magnetic material (M-Sp)

$FeCl_3$ (0.004 mol) and $FeSO_4 \cdot 7H_2O$ (0.003 mol) were each dissolved in 3 mL of distilled water and the solution was mixed using a stirrer for 3 h. Ammonia (3.5 mL of 25% solution) was then slowly dripped into the mixture. Subsequently, 1 g of Sp was added and stirred for 30 min. The mixture was then placed in a hydrothermal stainless-steel autoclave for 3 h at 150°C. Next, it was filtered and washed using distilled water, and dried in the oven at 100°C. The material was characterized using XRD, FTIR, VSM, and SEM-EDS analyses.

2.4 Preparation of hydrochar-based magnetic material (M-HSp)

$FeCl_3$ (0.004 mol) and $FeSO_4 \cdot 7H_2O$ (0.003 mol) were each dissolved in 25 mL of distilled water, and the solution was mixed and stirred using a stirrer for 3 h. Ammonia (3.5 mL of 25% solution) was then slowly dripped into the mixture, after which 1 g of the HSp was added and stirred for 30 min. Subsequently the mixture was placed in hydrothermal stainless-steel autoclave for 3 h at 150°C. It was then filtered and washed using distilled water, and then dried in the oven at 100°C. The obtained material was characterized using XRD, FTIR, VSM, and SEM-EDS analyses.

2.5 Adsorption process and regeneration ability

Adsorption was performed by considering several parameters, including the pH pzc, contact time, concentration, and temperature. The pH pzc was determined by varying the pH of the NaCl solution, and then adding 0.02 g of the material to the solution and stirring for 24 h, after which the final pH of the solution was measured. The effect of the contact time for the adsorption of MG dye was measured by varying the contact time during adsorption. As much as 0.02 g of the adsorbent was added to an Erlenmeyer flask containing 20 mL of the dye solution at a concentration of 50 mg/L. The mixture was stirred, following which the absorbance of the filtrate was measured using a UV-visible spectrophotometer for the specified time variation. The effects of the concentration and temperature were determined by varying these parameters during adsorption. As much as 0.02 g of the adsorbent was added to an Erlenmeyer flask containing 20 mL of the dye solution for a specified concentration variation and stirred for 60 min at the specified temperature; subsequently, the absorbance of the filtrate was measured. The regeneration ability of the adsorbent was determined by performing adsorption-desorption cycles, where the latter process was performed to remove the adsorbate from the adsorbent. For this, 0.1 of the adsorbent was added to the dye solution at a concentration of 50 mg/L. The mixture stirred for 2 h, and the absorbance of the filtrate was measured. Desorption was carried out using an ultrasonic system with a water bath. The adsorbent that subjected to desorption was dried and reused in the subsequent adsorption process.

3. RESULTS AND DISCUSSION

The initial material (Sp), and the prepared hydrochar and magnetic materials are shown in Figure 2. The initial material changes in color to black in HSp due to the hydrothermal carbonization treatment, while it changes to brown in the magnetic material, indicating the presence of iron. Figures 2(c) and 2(d), show the testing procedure for the magnetic material using an external magnet, confirming its successful preparation. The data in Table 1 show that the yield weight of the resulting material reaches 70-90%.

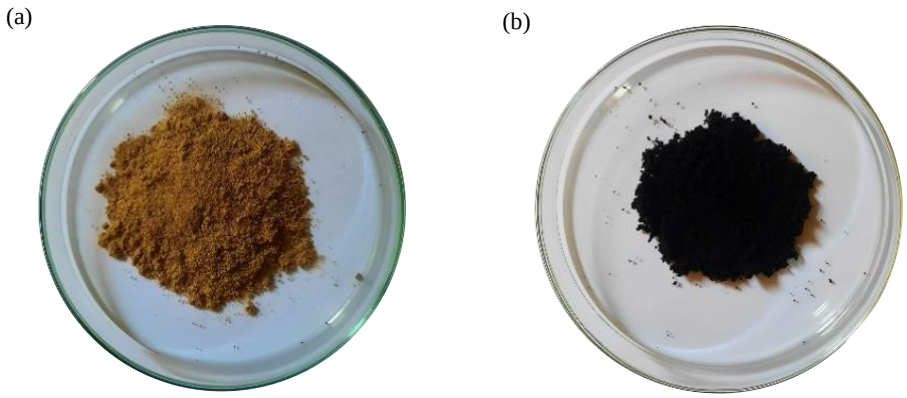

Figure 2. Materials of Sp (a), HSp (b), M-Sp (c), and M-HSp (d)

Figure 2. Materials of Sp (a), HSp (b), M-Sp (c), and M-HSp (d) (cont.)

Table 1. Percent yield weight of materials

Materials	Yield weight (%)
HSp	90.455
M-Sp	99.703
M-HSp	72.068

The XRD patterns of Sp, HSp, M-Sp, and M-HSp are shown in Figure 3. The patterns for Sp and HSp show diffraction peaks at 2θ≈=20º (002) indicating that these materials are amorphous with a low crystallinity (Venkatesan et al., 2022). The diffraction peaks of M-Sp and M-HSp are located at 2θ≈=20º (002), indicating the presence of the initial material; and peaks are also found at 2θ≈=30º (311), 35º (400), and 65º (440), originating from Magnetite (Chekalil et al., 2019).

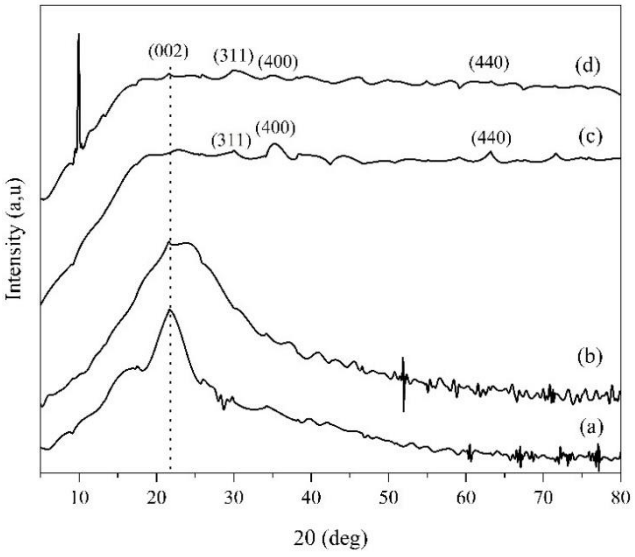

Figure 3. Diffraction patterns of Sp (a), HSp (b), M-Sp (c), and M-HSp (d)

The FT-IR spectra of Sp, HSp, M-Sp, and M-HSp are shown in Figure 4. The peak at 3,425 cm^{-1} is assigned to the O-H bond from the phenolic hydroxyl group, while the peaks at 2,924, 1,630, and 1,003 cm^{-1} correspond to the C-H, C=C, and C-O functional groups, respectively. The spectra of the M-Sp and M-HSp materials show a peak at 560 cm^{-1}, indicating the presence of the Fe-O bond. The magnetic curves of M-Sp and M-HSp were measured using VSM and are shown in Figure 5; both materials are paramagnetic with magnetizations of 17.69 emu/g and 5.65 emu/g, respectively. The hysteresis curve is at the null position, implying that M-Sp and M-HSp are superparamagnetic.

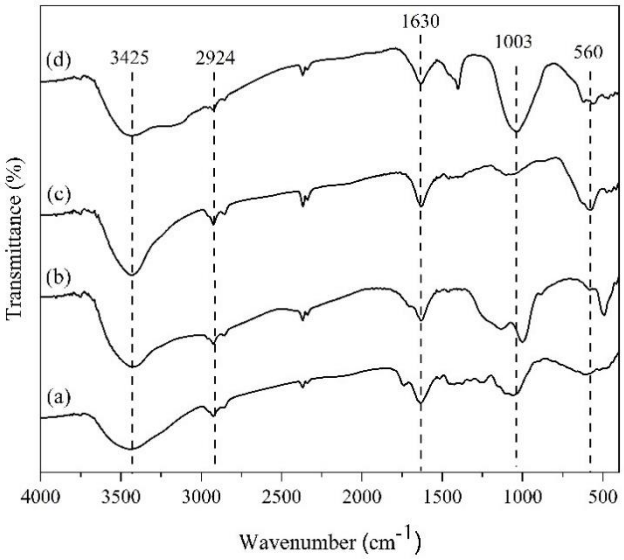

Figure 4. FT-IR Spectrum of Sp (a), HSp (b), M-Sp (c), and M-HSp (d)

The SEM–EDS results are shown in Figure 6 and Table 2. Figure 2 shows that the materials forms aggregates and is heterogeneous. Hsp and M-Hsp exhibit a smoother morphology than Sp and M-Sp. Table 2 show the EDS data with percentages of the C, O, and Fe atoms. HSp has a higher C content than Sp due to hydrothermal carbonization. This proves the

success of the hydrothermal carbonization treatment carried out in this study. M-Sp and M-HSp exhibit Fe content due to the magnetization process in the materials; M-Sp has a higher Fe content than M-Hsp. This is reflected in the magnetization of M-Sp, which is higher than that of M-HSp.

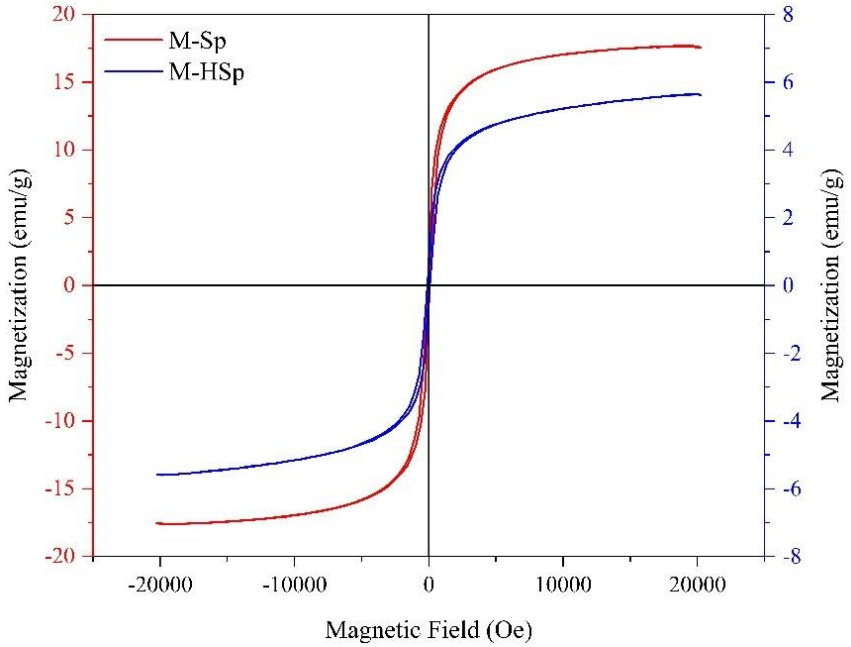

Figure 5. Magnetization curve

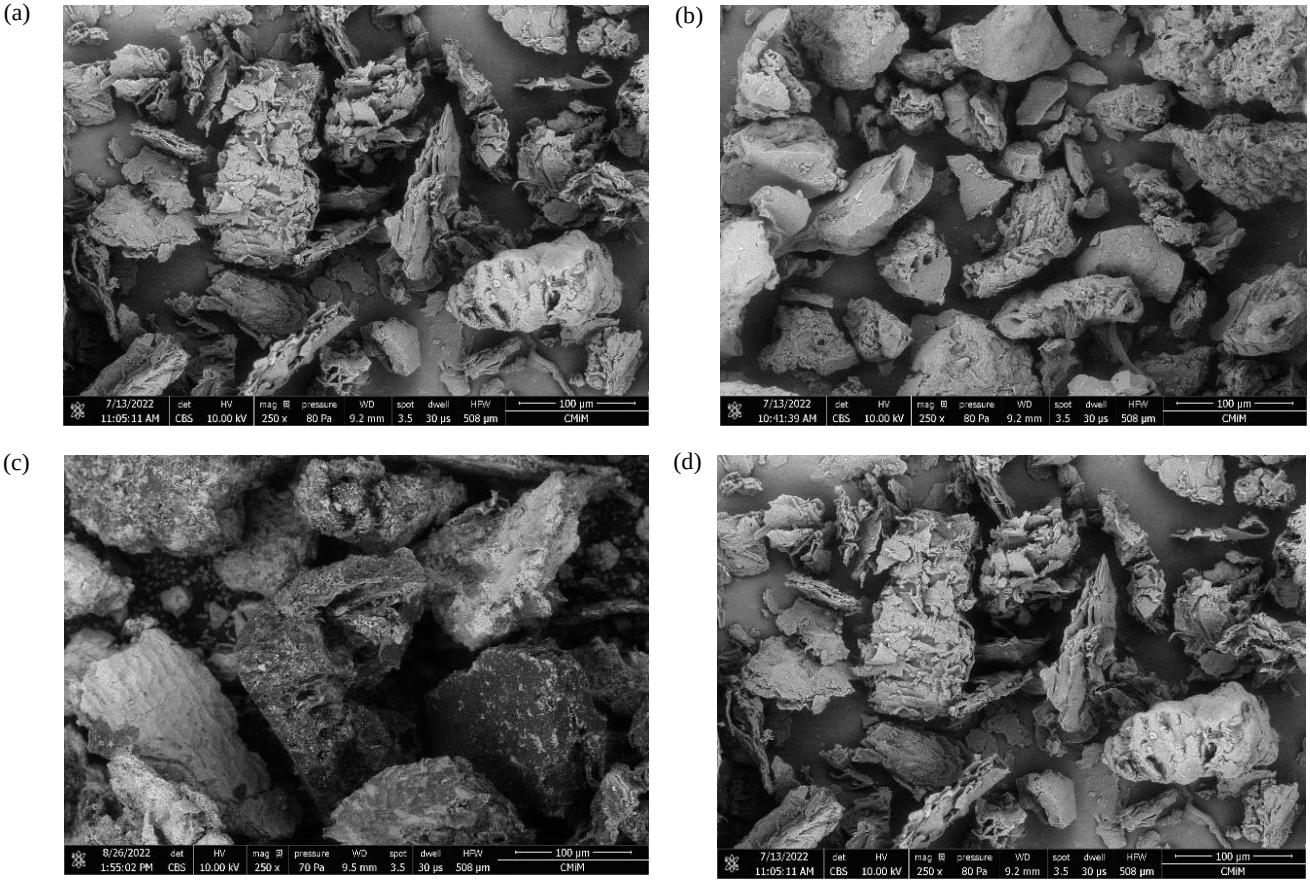

Figure 6. SEM images of Sp (a), Hsp (b), M-Sp (c), and M-Hsp (d)

Table 2. EDS data of materials

Materials	Weight (%)		
	C	O	Fe
Sp	55.9	32.8	-
HSp	68	26.3	-
M-Sp	17.7	31.6	46.9
M-HSp	18.2	34.6	36.4

The results of the pH pzc measurements are shown in Figure 7. The pH pzc of the materials is approximately in the range of 4.5-5.9. This implies that for this pH range, the material surfaces are neutral and carry zero charge, enabling optimal adsorption without the influence of positive or negative charges. The pH pzc of each material was evaluated for the adsorption of MG dye. The adsorption kinetic parameters are shown in Figure 8 and Table 3. The equilibrium adsorption of MG dye occurs at 90 min. Table 3 shows that the adsorption kinetics follow the PSO model, with a linear regression coefficient (R^2) close to 1. The kinetic rate of the PSO model is lower than of the PFO model, indicating that the reaction proceeds faster with the former model.

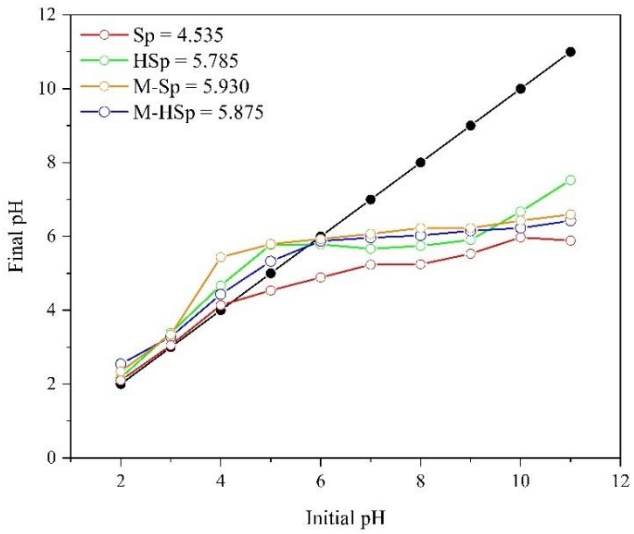

Figure 7. pH pzc of materials

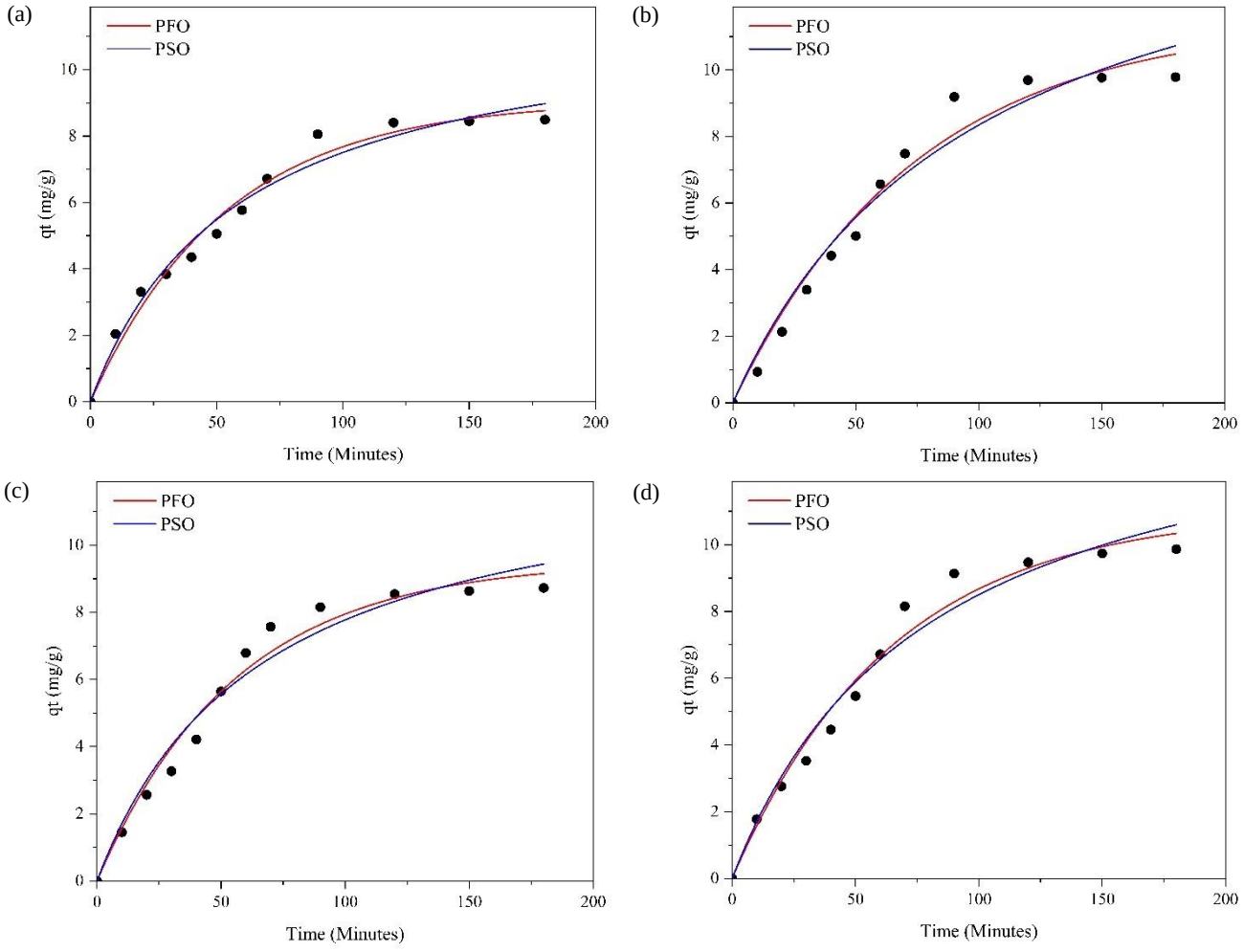

Figure 8. Adsorption kinetic models and equilibrium condition of Sp (a), HSp (b), M-Sp (c), and M-HSp (d)

Table 3. Adsorption kinetic parameters

Adsorbents	Initial concentration (mg/L)	$Qe_{experiment}$ (mg/g)	PFO			PSO		
			Qe_{Calc} (mg/g)	R^2	k1	Qe_{Calc} (mg/g)	R^2	k2
Sp	10.586	8.496	13.813	0.944	0.037	11.364	0.963	0.0017
HSp	10.586	9.785	22.930	0.926	0.044	16.155	0.900	0.0006
M-Sp	10.586	8.726	12.272	0.969	0.033	13.158	0.934	0.0010
M-HSp	10.586	9.867	13.868	0.971	0.030	15.337	0.937	0.0008

The adsorption isotherm models are shown in Figure 9 and Table 4, and indicate that the increasing temperature causes an increase in the adsorption concentration. The adsorption capacity of the materials is enhanced by the hydrothermal and magnetic treatments compared to that of the initial material. The adsorption capacities of Sp, HSp, M-Sp, and M-HSp are 66.667, 86.957, 69.444, and 88.889 mg/g, respectively. Based on isotherm data, the Langmuir model is better than the Freundlich model for the adsorption process in this study, with R^2 close to 1. The adsorption thermodynamic parameters are shown in Table 5. The adsorption process that occurs in this study is an endothermic process, as indicated by the positive ΔH; the ΔS value indicates the degree of irregularity of the adsorption process.

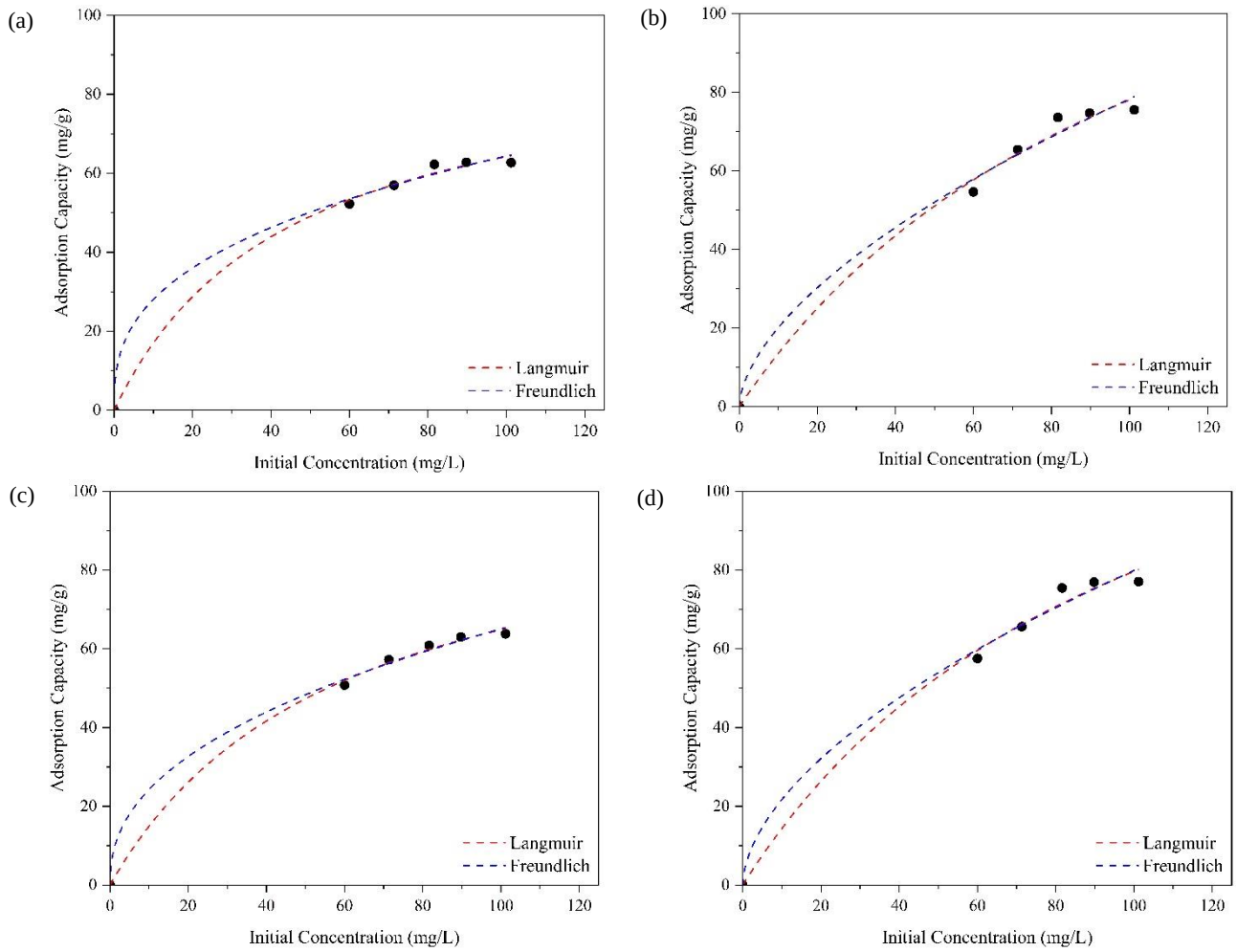

Figure 9. Adsorption isotherm models of Sp (a), HSp (b), M-Sp (c), and M-HSp (d)

Table 4. Adsorption isotherm parameters

Adsorbents	Adsorption isotherm	Adsorption constant	T (K)				
			30°C	40°C	50°C	60°C	70°C
Sp	Langmuir	Q_{max}	59.524	60.976	62.112	65.359	66.667
		kL	0.239	0.281	0.338	0.371	0.514
		R^2	0.996	0.998	0.998	0.997	0.998
	Freundlich	n	8.078	7.862	8.439	7.905	8.110
		kF	33.963	35.099	37.575	38.833	41.295
		R^2	0.870	0.939	0.935	0.859	0.863
HSp	Langmuir	Q_{max}	86.957	67.568	71.429	76.336	80.645
		kL	0.477	0.712	0.654	0.630	0.639
		R^2	0.999	0.999	0.998	0.996	0.994
	Freundlich	n	3.709	3.719	3.610	3.674	3.897
		kF	23.281	24.820	25.598	28.379	32.240
		R^2	0.858	0.882	0.936	0.992	0.995
M-Sp	Langmuir	Q_{max}	63.291	64.103	64.516	68.966	69.444
		kL	0.138	0.198	0.278	0.240	0.319
		R^2	0.992	0.990	0.997	0.999	0.999
	Freundlich	n	4.785	5.848	6.549	5.705	6.094
		kF	24.826	30.444	34.096	33.281	36.249
		R^2	0.894	0.816	0,909	0.967	0.924
M-HSp	Langmuir	Q_{max}	70.922	74.627	76.336	77.519	88.889
		kL	0.716	0.558	0.697	0.921	1.103
		R^2	0.999	0.998	0.996	0.997	0.998
	Freundlich	n	4.026	3.561	3.970	4.444	5.048
		kF	27.983	26.309	30.740	34.898	39.967
		R^2	0.991	0.958	0.999	0.999	0.996

Table 5. Adsorption thermodynamic parameters

Adsorbents	Concentration (mg/L)	T (K)	Q_e (mg/g)	ΔH (kJ/mol)	ΔS (J/mol. K)	ΔG (kJ/mol)
Sp	101.185 mg/L	303	54.926	6.990	0.024	-0.389
		313	56.481			-0.633
		323	58.111			-0.876
		333	60.889			-1.120
		343	62.704			-1.363
HSp	101.185 mg/L	303	62.296	13.070	0.047	-1.091
		313	64.926			-1.559
		323	67.778			-2.026
		333	71.592			-2.494
		343	75.555			-2.961
M-Sp	101.185 mg/L	303	54.704	8.186	0.045	-5.436
		313	57.285			-5.886
		323	58.926			-6.335
		333	62.259			-6.785
		343	63.815			-7.234
M-HSp	101.185 mg/L	303	67.370	9.714	0.038	-1.716
		313	70.111			-2.093
		323	72.000			-2.470
		333	73.889			-2.847
		343	77.074			-3.224

The regeneration ability of the material in Figure 10 shows that the initial material (Sp) can only be used for three regeneration cycles, while the materials subjected to the hydrothermal and magnetic treatments can be used for four regeneration cycles. Table 6 lists the adsorption capacities for reported magnetic materials. The table shows that the magnetic material prepared in this study has a higher adsorption capacity, rendering it promising for dye removal. Figure 11 illustrates the possible adsorption mechanism of MG dye by M-Sp and M-HSp, involving hydrogen bond, electrostatic, π-π, and physical interactions. It shows that the adsorption process of MG dye involves not only physical interactions, but also chemical interactions.

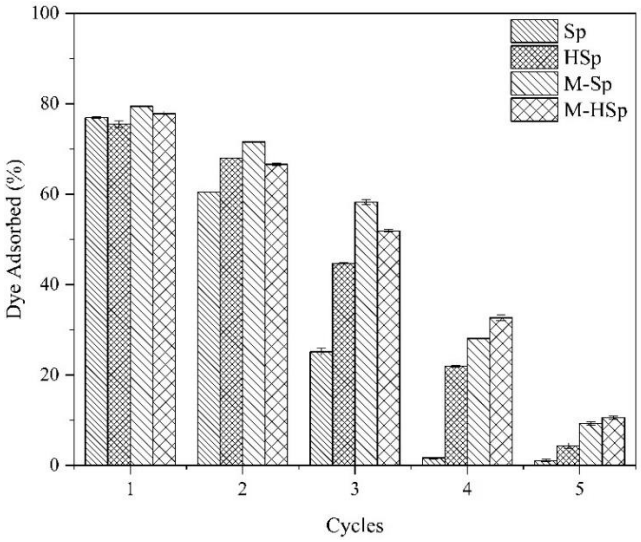

Figure 10. Regeneration ability of materials

Table 6. Comparison of several adsorbents on the adsorption of MG

Adsorbents	Adsorption capacity (mg/g)	Equilibrium time (minutes)	References
Fe_3O_4@chitosan@ZIF-8	3.282	40	Zadvarzi et al. (2021)
Polyaniline–nickel ferrite magnetic nanocomposite	4.09	210	Patil and Shrivastava (2015)
Magnetic $CuFe_2O_4$ nano-adsorbent	22	30	Vergis et al. (2018)
Sodium alginate-coated Fe_3O_4 nanoparticles	47.84	20	Mohammadi et al. (2014)
Magnetic GO/Fe_3O_4	59	90	Li et al. (2021)
Magnetic litchi pericarps	70.42	60	Zheng et al. (2015)
Cobalt ferrite silica magnetic nanocomposite	75.5	40	Amiri et al. (2017)
Magnetic reduced graphene oxide nanocomposite	77.15	20	Sadegh et al. (2021)
Magnetic chitosan-DES nanoparticles	87.72	120	Sadiq et al. (2021)
M-Sp	69.444	90	This work
M-HSp	88.889	90	This work

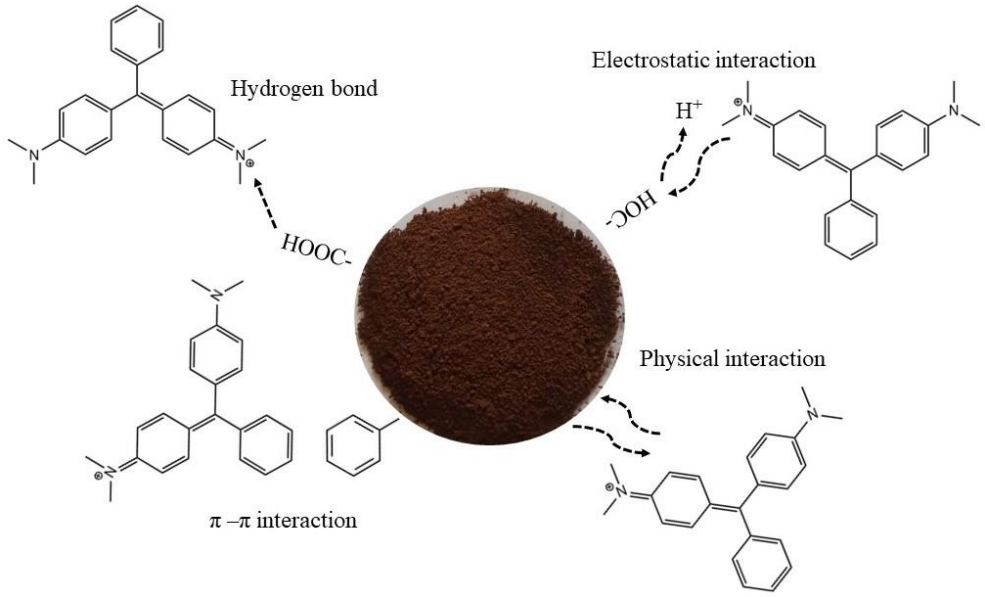

Figure 11. Plausible adsorption mechanism of MG by M-Sp and M-HSp

4. CONCLUSION

In this study, fruit-peel-based magnetic materials (M-Sp and M-HSp) were successfully synthesized by hydrothermal and magnetization treatments. The materials were used as adsorbents for the removal of MG dye. Equilibrium adsorption occurred at 90 min; the adsorption kinetics followed the PSO model and the adsorption isotherm fitted well to the Langmuir isotherm. The adsorption capacities of M-Sp and M-HSp were 69.444 and 88.889 mg/g, respectively. The adsorbent reusabilities of M-Sp and M-HSp were high, and both materials could be reused for up to four regeneration cycles compared to the three cycles for the untreated initial material. The adsorption mechanism of MG by M-Sp and M-HSp was suggested to involve hydrogen bonds, electrostatic, π-π, and physical interactions.

ACKNOWLEDGEMENTS

The authors acknowledge support by the Ministry of Education, Culture, Research and Technology Republic Indonesia through the Hibah Disertasi Doctor main contract number (142/E5/PG.02.00.PT/2022) by derivative contract number (0145.009/UN9.3.1/PL/2022). The authors also thank the Research Center of Inorganic Materials and Complexes, Universitas Sriwijaya for the analysis, apparatus, support, and discussion of this research.

REFERENCES

Alqadami AA, Khan MA, Siddiqui MR, Alothman ZA. Development of citric anhydride anchored mesoporous MOF through post synthesis modification to sequester potentially toxic lead (II) from water. Microporous and Mesoporous Materials 2018;261:198-206.

Amiri M, Salavati NM, Akbari A, Gholami T. Removal of malachite green (a toxic dye) from water by cobalt ferrite silica magnetic nanocomposite: Herbal and green sol-gel autocombustion synthesis. International Journal of Hydrogen Energy 2017;42(39):24846-60.

Azizah U, Fatimah I. Salacca zalacca skin and its modified form as biosorbents for Hg^{2+} removal from aqueous solution. Green Chemistry Letters and Reviews 2020;13(3):42-50.

Çatlıoğlu FN, Akay S, Gözmen B, Turunc E, Anastopoulos I, Kayan B, et al. Fe-modified hydrochar from orange peel as adsorbent of food colorant Brilliant Black: Process optimization and kinetic studies. International Journal of Environmental Science and Technology 2020;17(4):1975-90.

Chekalil N, Tarhini M, Elaissari A, Saïdi-Besbes S. Multi-step synthesis of core-shell magnetic nanoparticles bearing acid-chelating functional moieties. Research on Chemical Intermediates 2019;45(10):4847-61.

Cheng S, Zhao S, Xing B, Liu Y, Zhang C, Xia H. Preparation of magnetic adsorbent-photocatalyst composites for dye removal by synergistic effect of adsorption and photocatalysis. Journal of Cleaner Production 2022;348(3):Article No. 131301.

Cojocaru C, Samoila P, Pascariu P. Chitosan-based magnetic adsorbent for removal of water-soluble anionic dye: Artificial neural network modeling and molecular docking insights. International Journal of Biological Macromolecules 2019; 123:587-99.

Das P, Debnath P, Debnath A. Enhanced sono-assisted adsorptive uptake of malachite green dye onto magnesium ferrite nanoparticles: Kinetic, isotherm and cost analysis. Environmental Nanotechnology, Monitoring and Management 2021;16:Article No. 100506.

Dil AA, Vafaei A, Ghaedi AM, Ghaedi M, Dil EA. Multi-responses optimization of simultaneous adsorption of methylene blue and malachite green dyes in binary aqueous system onto Ni:FeO(OH)-NWs-AC using experimental design: Derivative spectrophotometry method. Applied Organometallic Chemistry 2018;32(3):1-13.

Gajera R, Vardhan R, Yadav A, Kumar P. Adsorption of cationic and anionic dyes on photocatalytic flyash/TiO_2 modified chitosan biopolymer composite. Journal of Water Process Engineering 2022;49(7):Article No. 102993.

Haris M, Khan MW, Paz-Ferreiro J, Mahmood N, Eshtiaghi N. Synthesis of functional hydrochar from olive waste for simultaneous removal of azo and non-azo dyes from water. Chemical Engineering Journal Advances 2022;9:Article No. 100233.

Hasanah M, Wijaya A, Arsyad FS, Mohadi R, Lesbani A. Preparation of hydrochar from *Salacca zalacca* peels by hydrothermal carbonization: Study of adsorption on congo red dyes and regeneration ability. Science and Technology Indonesia 2022;7(3):372-8.

Karthi S, Sangeetha RK, Arumugam K, Karthika T, Vimala S. Removal of methylene blue dye using shrimp shell chitin from industrial effluents. Materials Today: Proceedings 2022; 5:Article No. 428.

Kaveh R, Bagherzadeh M. Simultaneous removal of mercury ions and cationic and anionic dyes from aqueous solution using epichlorohydrin cross-linked chitosan@magnetic Fe_3O_4/ activated carbon nanocomposite as an adsorbent. Diamond and Related Materials 2022;124(2):Article No. 108923.

Li W, Xu M, Cao Q, Luo J, Yang S, Zhao G. Magnetic GO/Fe_3O_4 for rapid malachite green (MG) removal from aqueous solutions: A reversible adsorption. RSC Advances 2021; 11(32):19387-94.

Ling C, Yimin D, Qi L, Chengqian F, Zhiheng W, Yaqi L, et al. Novel High-efficiency adsorbent consisting of magnetic cellulose-based ionic liquid for removal of anionic dyes. Journal of Molecular Liquids 2022;353:Article No. 118723.

Mohadi R, Normah N, Fitri ES, Palapa NR. Unique adsorption properties of cationic dyes malachite green and rhodamine-B on longan (*Dimocarpus longan*) peel. Science and Technology Indonesia 2022;7(1):115-25.

Mohammadi A, Daemi H, Barikani M. Fast removal of malachite green dye using novel superparamagnetic sodium alginate-coated Fe_3O_4 nanoparticles. International Journal of Biological Macromolecules 2014;69:447-55.

Patil MR, Shrivastava VS. Adsorption of malachite green by polyaniline-nickel ferrite magnetic nanocomposite: An isotherm and kinetic study. Applied Nanoscience (Switzerland) 2015;5(7):809-16.

Qiao Q, Zhou H, Guo F, Shu R, Liu S, Xu L, et al. Facile and scalable synthesis of mesoporous composite materials from coal gasification fine slag for enhanced adsorption of malachite green. Journal of Cleaner Production 2022; 22(110):Article No. 131932.

Rahmayanti A, Firdaus A, Tamyiz M, Hamidah LN, Oktavia L, Rosyidah E, et al. Synthesis and effectiveness of snake fruit (*Salacca zalacca*) seed charcoal bio-adsorbent in reducing remazol brilliant blue. IOP Conference Series: Earth and Environmental Science 2022;1030(1):Article No. 012016.

Sadegh N, Haddadi H, Arabkhani P, Asfaram A, Sadegh F. Simultaneous elimination of rhodamine B and malachite green dyes from the aqueous sample with magnetic reduced graphene oxide nanocomposite: Optimization using experimental design. Journal of Molecular Liquids 2021; 343:Article No. 117710.

Sadiq AC, Olasupo A, Rahim NY, Ngah WSW, Suah FBM. Comparative removal of malachite green dye from aqueous solution using deep eutectic solvents modified magnetic chitosan nanoparticles and modified protonated chitosan beads. Journal of Environmental Chemical Engineering 2021;9(5):Article No. 106281.

Sanad MMS, Farahat MM, Abdel KMA. One-step processing of low-cost and superb natural magnetic adsorbent: Kinetics and thermodynamics investigation for dye removal from textile wastewater. Advanced Powder Technology 2021;32(5): 1573-83.

Venkatesan S, Ahmed H, Ali I, Rafique N. Evaluation of the production of hydrochar from spent coffee grounds under different operating conditions. Journal of Water Process Engineering 2022;49(7):Article No. 103037.

Vergis BR, Hari KR, Kottam N, Nagabhushana BM, Sharath R, Darukaprasad B. Removal of malachite green from aqueous solution by magnetic $CuFe_2O_4$ nano-adsorbent synthesized by one pot solution combustion method. Journal of Nanostructure in Chemistry 2018;8(1):1-12.

Wang Z, Ren D, Zhang X, Zhang S, Chen W. Adsorption-degradation of malachite green using alkali-modified biochar immobilized laccase under multi-methods. Advanced Powder Technology 2022;33(11):Article No. 103821.

Wu J, Yang J, Feng P, Wen L, Huang G, Xu C, et al. Highly efficient and ultra-rapid adsorption of malachite green by recyclable crab shell biochar. Journal of Industrial and Engineering Chemistry 2022;113:206-14.

Yvonne KS, Mahani Y, Razak W, Sofiyah MR, Razali MH. Properties of epoxy-hybrid composite using bamboo fiber and *Salacca zalacca* fruit skin powder. Materials Today: Proceedings 2018;5(10):21759-64.

Zadvarzi SB, Khavarpour M, Vahdat SM, Baghbanian SM, Rad AS. Synthesis of Fe_3O_4@chitosan@ZIF-8 towards removal of malachite green from aqueous solution: Theoretical and experimental studies. International Journal of Biological Macromolecules 2021;168:428-41.

Zheng H, Qi J, Jiang R, Gao Y, Li X. Adsorption of malachite green by magnetic litchi pericarps: A response surface methodology investigation. Journal of Environmental Management 2015;162:232-9.

Zubaidah E, Dewantari FJ, Novitasari FR, Srianta I, Blanc PJ. Potential of snake fruit (*Salacca zalacca* (Gaerth.) Voss) for the development of a beverage through fermentation with the *Kombucha consortium*. Biocatalysis and Agricultural Biotechnology 2018;13(9):198-203.